Linear instability of two-dimensional low-amplitude gap solitons near band edges in periodic media

Zuoqiang Shi,[1] Jiandong Wang,[2] Zhigang Chen,[3] and Jianke Yang[2,*]
[1]*Zhou Pei-Yuan Center for Applied Mathematics, Tsinghua University, Beijing 100084, China*
[2]*Department of Mathematics and Statistics, University of Vermont, Burlington, Vermont 05401, USA*
[3]*Department of Physics and Astronomy, San Francisco State University, San Francisco, California 94132, USA*
(Received 30 September 2008; published 5 December 2008)

Previous work has shown that in a two-dimensional periodic medium under focusing or defocusing cubic nonlinearities, gap solitons in the form of low-amplitude and slowly modulated single-Bloch-wave packets can bifurcate out from the edges of Bloch bands. In this paper, linear stability properties of these gap solitons near band edges are determined both analytically and numerically. Through asymptotic analysis, it is shown that these gap solitons are linearly unstable if the slope of their power curve at the band edge has the opposite sign of nonlinearity (here focusing nonlinearity is said to have a positive sign, and defocusing nonlinearity to have a negative sign). An equivalent condition for linear instability is that the power of the gap solitons near the band edge is lower than the limit power value on the band edge. Through numerical computations of the power curves, it is found that this condition is always satisfied, thus two-dimensional gap solitons near band edges are linearly unstable. The analytical formula for the unstable eigenvalue of gap solitons near band edges is also asymptotically derived. It is shown that this unstable eigenvalue is proportional to the cubic power of the soliton's amplitude, and it induces width instabilities of gap solitons. A comparison between this analytical eigenvalue formula and numerically computed eigenvalues shows excellent agreement.

DOI: 10.1103/PhysRevA.78.063812 PACS number(s): 42.65.Tg, 05.45.Yv

I. INTRODUCTION

Nonlinear wave phenomena in periodic media are receiving intensive studies in many branches of science and engineering these days. Two prominent examples are nonlinear optics and Bose-Einstein condensates. In nonlinear optics, a periodic medium can be created by sophisticated fabrication techniques [1,2], by laser writing [3,4], or by optical induction techniques [5–7]. In Bose-Einstein condensates, a periodic trapping potential for the condensates can be introduced by laser beams [8]. The motivation for the study of nonlinear wave phenomena in these periodic media is that the periodic media exhibit very novel dispersion (or diffraction) behaviors—most notably the appearance of band gaps inside the continuous spectrum [1,9]. These novel dispersion (diffraction) behaviors, when coupled with self-focusing or self-defocusing nonlinearity, give rise to new types of self-trapped localized states (gap solitons), which reside either in the semi-infinite band gap or higher band gaps [5,10], and these gap solitons can be utilized for various applications [8,12]. So far, a wide variety of gap solitons have been reported either theoretically, or experimentally, or both. They include fundamental and vortex solitons in the semi-infinite gap (under focusing nonlinearity) [2,5,13–16], fundamental and vortex solitons in the first gap (under defocusing nonlinearity) [5,17,18], reduced-symmetry solitons and vortex-array solitons in the first gap (under focusing nonlinearity) [19,20], gap-wave solitons in the first gap (under defocusing nonlinearity) [8,11], embedded soliton trains (under either focusing or defocusing nonlinearity) [21], etc. Solitons in ring lattices and quasiperiodic lattices have been explored as well [22–24]. Analytically one-dimensional (1D) gap solitons bifurcating from edges of Bloch bands were investigated in [25]. It was found that the centers of such 1D gap solitons can only be at two locations. One location is at a potential minimum (also called a lattice site), and such a soliton is referred to as an on-site soliton. The other location is between lattice sites, and such a soliton is referred to as an off-site soliton [26]. In two dimensions, classifications of gap solitons bifurcating from edges of Bloch bands were performed in [10]. It was found that the centers of two-dimensional (2D) gap solitons can only be at four locations: one is on site, and the other three are off site. More importantly, it was revealed that near band edges with two Bloch modes, the coupling between these Bloch modes gives rise to many new types of gap solitons such as reduced-symmetry solitons [19] and vortex-array solitons [20]). It has also been recognized that some gap solitons (such as vortex solitons [13,18]) do not bifurcate from the edges of Bloch bands [27,28].

Stability of gap solitons with respect to perturbations is an important issue, because only stable solitons are promising for experimental observations and physical applications. An important criterion for the linear stability of solitary waves is the Vakhitov-Kolokolov (VK) stability criterion, which says that under a certain spectral condition, sign-definite solitary waves are linearly unstable if and only if the slope of the power curve is negative [29–34] (a related criterion in terms of the Hamiltonian-power diagram for homogeneous media was given in [35]). Most gap solitons, however, are not sign definite, thus the VK criterion does not apply. Because of that, other methods need to be developed. In one dimension, asymptotic analysis has been carried out for the linear stability of low-amplitude gap solitons near band edges [25]. It has been shown that on-site gap solitons near band edges can be

*Corresponding author; jyang@math.uvm.edu

linearly stable, while off-site solitons near band edges are always linearly unstable due to drift instabilities induced by translational-mode-related unstable eigenvalues [25]. Away from band edges, additional instabilities can also arise. In two dimensions, however, our knowledge on the stability of gap solitons is much more limited. It is well known that stability properties of solitary waves strongly depend on the number of spatial dimensions. Thus 1D stability results may not be carried over to the 2D case. Some limited stability results of gap solitons have been obtained in two dimensions recently. For instance, in the semi-infinite band gap under focusing cubic nonlinearity, it has been shown numerically that 2D on-site solitons are linearly stable away from the band edge where the power curve has a positive slope, but are linearly unstable near the band edge where the power curve has a negative slope [13]. This result can be readily explained analytically by the VK stability criterion since these gap solitons are sign definite [29–34] (note that the propagation constant in [13] was defined with the opposite sign of that in [29,33]; in this paper we follow the definition of [29,33]). For certain sign-indefinite gap solitons, limited numerical stability analysis has been performed as well (for instance, on out-of-phase dipole solitons and vortex solitons) [13,36–38]. It was found that such solitons may be stable in certain parameter regions. But stability properties of many other sign-indefinite gap solitons, especially in higher band gaps, are still unknown.

In this paper, we analytically determine the stability properties of 2D gap solitons near edges of Bloch bands in a sinusoidal lattice potential under either the focusing or defocusing cubic (Kerr) nonlinearity by asymptotic methods. These gap solitons are low-amplitude slowly modulated *single*-Bloch-wave packets. We show that these solitons are linearly unstable if the slope of their power curve at the band edge has the opposite sign of the nonlinearity. Specifically, these gap solitons near a band edge are linearly unstable if the power curve has a negative slope under the focusing nonlinearity, or if the power curve has a positive slope under the defocusing nonlinearity. This result generalizes and modifies the VK stability criterion to sign-indefinite gap solitons, and it reveals the important role the sign of nonlinearity plays in the connection between linear stability and the power slope. An equivalent condition for linear instability of 2D gap solitons near band edges is that the powers of these solitons near band edges are lower than the limit power values on the band edges. Our numerical computations of the power curves near many band edges indicate that this instability condition is all satisfied for both on-site and off-site gap solitons, thus these 2D gap solitons near band edges are linearly unstable. This contrasts the one-dimensional case where on-site gap solitons near band edges can be linearly stable [25]. The asymptotic expression for the unstable eigenvalue of 2D gap solitons near band edges is also derived. We find that this unstable eigenvalue bifurcates from the eigenmode of the 2D envelope soliton's zero eigenvalue induced by this envelope soliton's variation with respect to its propagation constant. This eigenmode with zero eigenvalue for the 2D envelope soliton does not exist in one dimension, thus this unstable eigenvalue of 2D gap solitons has no counterpart in the 1D case. We also show that this unstable eigenvalue leads to width instabilities of 2D gap solitons, and its magnitude is proportional to the cubic power of the soliton's amplitude. Lastly, the asymptotic expression for this unstable eigenvalue is compared with numerically computed eigenvalues for both the focusing and defocusing nonlinearities, and excellent agreement is obtained. We point out that our instability results of 2D gap solitons near band edges do not conflict with experimental observations of such solitons in [5,17,19] because the observed solitons have high amplitudes and do not reside near band edges.

II. LOW-AMPLITUDE 2D GAP SOLITONS NEAR BAND EDGES

The mathematical model we consider is the 2D nonlinear Schrödinger (NLS) equation with a periodic potential as follows:

$$iU_t + U_{xx} + U_{yy} - V(x,y)U + \sigma|U|^2U = 0, \tag{2.1}$$

where $U(x,y,t)$ is a complex function, the potential $V(x,y)$ is periodic in x and y (it is also called a lattice potential), and $\sigma = \pm 1$ is the sign of nonlinearity. When $\sigma=1$, the nonlinearity is of self-focusing type, while when $\sigma=-1$, the nonlinearity is of self-defocusing type. This model arises in Bose-Einstein condensates trapped in a 2D optical lattice (where t is time) [18,39] as well as light propagation in a periodic Kerr medium under paraxial approximation (where t is the distance of propagation). In certain optical materials (such as photorefractive crystals), the nonlinearity is of a different (saturable) type. But those different nonlinearities often give qualitatively similar results as the cubic nonlinearities above in a periodic lattice [13,15,16,36].

In this paper we take the lattice potential as

$$V(x,y) = V_0(\sin^2 x + \sin^2 y), \tag{2.2}$$

whose periods along the x and y directions are both equal to π. This square-lattice potential can be readily engineered in Bose-Einstein condensates [8,18] and optics [5,6]. This potential is separable, which makes our theoretical analysis a little easier. Similar analysis can be repeated for other types of periodic potentials with minimal changes.

Gap solitons in Eq. (2.1) are sought in the form

$$U(x,y,t) = u(x,y)e^{i\mu t}, \tag{2.3}$$

where the amplitude function $u(x,y)$ is real valued and satisfies the following equation:

$$u_{xx} + u_{yy} - [F(x) + F(y)]u - \mu u + \sigma u^3 = 0. \tag{2.4}$$

Here $F(x) = V_0 \sin^2 x$, and μ is a propagation constant. Note that the propagation constant in the above definition is the same as that in most papers on the stability theory of solitary waves in NLS-type equations [29,33]. This is convenient for the comparison between our stability results in this paper and those in previous papers. In our previous publications on 2D gap solitons [10,13], the propagation constant was defined with the opposite sign of that above. This should be kept in mind when quoting the results of [10,13].

When the amplitude of the gap soliton is infinitesimal, the nonlinear term in Eq. (2.4) drops out. Solutions of the re-

maining linear equation are Bloch modes, and the corresponding propagation constants form Bloch bands. Between Bloch bands, band gaps may appear if the lattice potential is strong enough (see [10] for details). When the amplitude of a gap soliton is small but not infinitesimal, the propagation constant lies near an edge of a Bloch band (inside a band gap), and the gap soliton is a slowly modulated packet of the Bloch wave at this band edge. In this paper, we consider the stability properties of low-amplitude 2D gap solitons near edges of Bloch bands. We restrict ourselves to gap solitons that are slowly modulated *single*-Bloch-wave packets. At some band edges where two linearly independent Bloch modes exist, nonlinear coupling between the two Bloch-wave packets could generate more complex gap solitons such as vortex-array solitons and dipole-array solitons [10,20]. Such solitons consisting of two Bloch-wave packets are excluded from discussion in this paper.

Below we determine single-Bloch-wave packet solitons near a band edge μ_0. This derivation is a special case of our more general derivation in [10] (see also [40]), and is thus only summarized here. This summary and proper extension are needed for the stability analysis in the next section.

Since the potential $V(x,y)$ is separable, a Bloch wave at this band edge has the form $p_1(x)p_2(y)$, where $p_{1,2}(x)$ are 1D Bloch waves at 1D band edges $\omega_{1,2}$ with

$$p_n'' - F(x)p_n - \omega_n p_n = 0, \quad n = 1,2, \tag{2.5}$$

and $\mu_0 = \omega_1 + \omega_2$. The first few 1D band-edge values ω_n and profiles of the corresponding Bloch waves $p_n(x)$ have been displayed in [10] (for $V_0 = 6$). These 1D Bloch functions have either period π or 2π depending on the band edge, and $p_n(x+\pi) = \pm p_n(x)$. Since the sinusoidal potential $F(x)$ is symmetric, Bloch functions $p_n(x)$ are either symmetric or antisymmetric, i.e., $p_n(-x) = \pm p_n(x)$. Gap solitons in the form of a low-amplitude and slowly modulated packet of the Bloch wave $p_1(x)p_2(y)$ have the following asymptotic expansions:

$$u = \epsilon u_0 + \epsilon^2 u_1 + \epsilon^3 u_2 + \cdots, \tag{2.6}$$

and

$$\mu = \mu_0 + \tau\epsilon^2, \tag{2.7}$$

where $\epsilon \ll 1$ is a soliton amplitude parameter,

$$u_0 = A(X,Y)p_1(x)p_2(y) \tag{2.8}$$

is the leading-order solution, $A(X,Y)$ is a real-valued slowly varying envelope function,

$$X = \epsilon(x - x_0), \quad Y = \epsilon(y - y_0) \tag{2.9}$$

are slow spatial variables, and (x_0, y_0) is the center position of the envelope function. In order to simplify notations, we define the following operator:

$$\mathcal{L}_0 = \frac{\partial^2}{\partial x^2} + \frac{\partial^2}{\partial y^2} - [F(x) + F(y)] - \mu + \sigma u^2(x,y), \tag{2.10}$$

then the solitary wave equation (2.4) becomes

$$\mathcal{L}_0 u(x,y) = 0. \tag{2.11}$$

Since function $u(x,y)$ contains fast and slow variables (x,y) and (X,Y), in our multiscale asymptotic analysis below, it is necessary to separate derivatives to these fast and slow variables in $\mathcal{L}_0$, so that $\mathcal{L}_0$ is rewritten as

$$\mathcal{L}_0 = M_0 + \epsilon M_1 + \epsilon^2 M_2 + \epsilon^2 \sigma(u_0 + \epsilon u_1 + \cdots)^2, \tag{2.12}$$

where

$$M_0 = \frac{\partial^2}{\partial x^2} + \frac{\partial^2}{\partial y^2} - [F(x) + F(y)] - \mu_0, \tag{2.13}$$

$$M_1 = 2\left(\frac{\partial^2}{\partial x \partial X} + \frac{\partial^2}{\partial y \partial Y}\right), \tag{2.14}$$

$$M_2 = \frac{\partial^2}{\partial X^2} + \frac{\partial^2}{\partial Y^2} - \tau. \tag{2.15}$$

Here the partial derivatives to x and y in M_0 and M_1 are with respect to the fast variables x and y only. Substituting the expansions (2.6) and (2.12) into the solitary wave equation (2.11), we get the following equations for the solutions u_n at various orders of ϵ:

$$\epsilon^1: \quad M_0 u_0 = 0, \tag{2.16}$$

$$\epsilon^2: \quad M_0 u_1 = -M_1 u_0, \tag{2.17}$$

$$\epsilon^3: \quad M_0 u_2 = -M_1 u_1 - (M_2 + \sigma u_0^2)u_0, \tag{2.18}$$

$$\epsilon^4: \quad M_0 u_3 = -M_1 u_2 - (M_2 + 3\sigma u_0^2)u_1, \tag{2.19}$$

$$\epsilon^5: \quad M_0 u_4 = -M_1 u_3 - (M_2 + 3\sigma u_0^2)u_2 - 3\sigma u_0 u_1^2. \tag{2.20}$$

The first-order equation (2.16) is satisfied automatically. The second-order equation (2.17) satisfies the Fredholm condition, i.e., its inhomogeneous periodic term $M_1 u_0$ (in fast variables x and y) is orthogonal to the homogeneous periodic solution $p_1(x)p_2(y)$ over a period of functions $p_1(x)$ and $p_2(y)$.

$$\int_0^{2\pi}\int_0^{2\pi} p_1(x)p_2(y)M_1 u_0 dxdy = 0. \tag{2.21}$$

Here the upper limits are taken as 2π rather than π because Bloch functions $p_{1,2}(x)$ may have period 2π rather than π (see above). Hence Eq. (2.17) admits a periodic solution, which is found to be

$$u_1 = \frac{\partial A}{\partial X}\nu_1(x)p_2(y) + \frac{\partial A}{\partial Y}p_1(x)\nu_2(y), \tag{2.22}$$

where $\nu_n(x)$ is the periodic solution of the equation

$$\nu_n'' - F(x)\nu_n - \omega_n \nu_n = -2p_n'(x), \quad n = 1,2. \tag{2.23}$$

To make $\nu_n(x)$ unique, we require its symmetry to be the same as that of $p_n'(x)$, i.e., the opposite of that of $p_n(x)$. Here

we did not add to u_1 the homogeneous solution of Eq. (2.17). The reason is that this homogeneous solution of Eq. (2.17) is of the form $B(X,Y)p_1(x)p_2(y)$. If this term were added to u_1 in Eq. (2.22), then the u_2 solution would contain terms with the same symmetry of $p_1(x)p_2(y)$ in fast (x,y) variables, plus the term $B_X\nu_1(x)p_2(y)+B_Yp_1(x)\nu_2(y)$. By using the Fredholm condition of the u_3 equation (2.19) and the symmetry properties of individual terms in fast variables as well as the relation (2.27), we would find that $\mathcal{L}_1^eB=0$, where operator $\mathcal{L}_1^e$ is defined in Eq. (3.21). Hence the B function would be a linear combination of A_X and A_Y in the view that function A satisfies Eq. (2.24). Then the resulting term $B(X,Y)p_1(x)p_2(y)$ could be lumped into the leading-order term u_0 by slightly shifting the center position of $A(X,Y)$, and thus could be removed from u_1. Now we insert the above expressions of u_0 and u_1 into the u_2 equation (2.18). In order for this u_2 equation to admit a bounded (periodic) solution in fast variables x and y, the Fredholm condition gives the envelope equation for $A(X,Y)$ as [10]

$$D_1\frac{\partial^2 A}{\partial X^2}+D_2\frac{\partial^2 A}{\partial Y^2}+\tau A-\sigma\alpha_0A^3=0, \tag{2.24}$$

where

$$D_n\equiv\left.\frac{1}{2}\frac{d^2\omega}{dk^2}\right|_{\omega=\omega_n},\quad n=1,2, \tag{2.25}$$

are the second-order dispersion coefficients at 1D band edges ω_n, and

$$\alpha_0=\frac{\int_0^\pi\int_0^\pi p_1^4(x)p_2^4(y)dxdy}{\int_0^\pi\int_0^\pi p_1^2(x)p_2^2(y)dxdy}>0. \tag{2.26}$$

In this derivation, we have used the relation [10,25]

$$\int_0^\pi[2\nu_n'(x)+p_n(x)]p_n(x)dx=-D_n\int_0^\pi p_n^2(x)dx, \tag{2.27}$$

where $n=1,2$. In the integrals of Eqs. (2.26) and (2.27), the upper limits are taken as π rather than 2π of [10] since the integrands here are periodic functions with period π even when the Bloch functions $p_{1,2}(x)$ have period 2π.

The envelope equation (2.24) is the familiar 2D NLS equation with constant coefficients. For the existence of gap solitons, the envelope function A must be a solitary wave, which decays to zero as (X,Y) approaches infinity. This requires that

$$\mathrm{sgn}(D_{1,2})=-\mathrm{sgn}(\sigma)=-\mathrm{sgn}(\tau). \tag{2.28}$$

Under these conditions, the envelope equation (2.24) admits a sign-definite ground-state 2D solitary wave which is bell shaped (also called Townes profile). It also admits other types of excited-state solutions such as vortices. In this paper, we only consider the ground-state solitary wave solution of the envelope equation (2.24). This ground-state envelope solution leads to the simplest gap-soliton solutions in the lattice system (2.4).

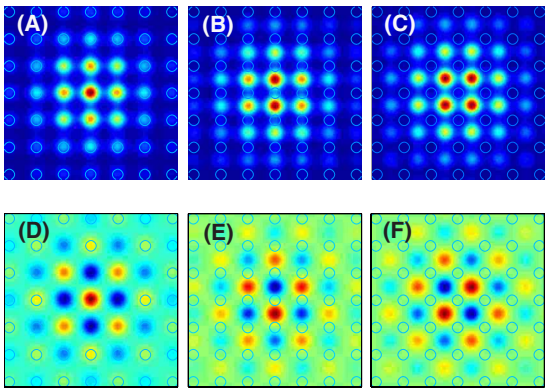

FIG. 1. (Color online) Upper row: three gap solitons near the right edge of the first Bloch band (with focusing nonlinearity), where all the intensity peaks of solitons are in phase with each other. Lower row: three gap solitons near the left edge of the first band (with defocusing nonlinearity), where adjacent intensity peaks of solitons are out of phase with each other. The propagation constants of these solitons are marked as red circles in the power curves of Fig. 2. Circles on the background here represent locations of lattice sites. Some circles in (A) and (D) are skipped to show the solitons better. [(A) and (D)] On-site gap solitons. [(B), (C), (E), and (F)] Off-site gap solitons.

It must be pointed out that at some 2D band edges with two linearly independent Bloch modes, the two Bloch modes can resonate with each other. In such cases, single-Bloch-wave packet solitons cannot exist (see band edge E in [10]).

The envelope equation (2.24) has constant coefficients. Thus it seems to suggest that the center of the envelope function A can move about freely in the (x,y) plane. This is not so, however. We have shown in [10] that due to an additional constraint on the solution, the center of the envelope function can only be located at four locations of the 2D lattice,

$$(x_0,y_0)=(0,0),\left(0,\frac{\pi}{2}\right),\left(\frac{\pi}{2},0\right),\left(\frac{\pi}{2},\frac{\pi}{2}\right). \tag{2.29}$$

The first location $(x_0,y_0)=(0,0)$ is at a lattice site [minimum of potential $V(x,y)$], hence the corresponding gap soliton is called an on-site soliton. The other locations are between lattice sites and correspond to off-site solitons. Notice that the second and third locations are equivalent to each other due to the symmetry of the lattice, thus they will be treated as the same. For illustration purposes, these three types of gap solitons near the two edges of the first Bloch band under focusing and defocusing nonlinearities are displayed in the upper and lower rows of Fig. 1, respectively (with $V_0=6$). Their propagation constants are marked by circles in Fig. 2. We see that in both cases, on-site solitons have a single intensity peak (maximum), while off-site solitons have two or four equal intensity peaks. The difference between focusing and defocusing nonlinearities is that under focusing nonlinearity (in the semi-infinite band gap), those intensity peaks are all in phase (see the upper row of Fig. 1), while under defocusing nonlinearity (in the first band gap), the intensity

peaks are out of phase between adjacent sites (see the lower row of Fig. 1).

The power curve of gap solitons near band edges will prove to be very important in our stability analysis of the next section. Indeed, for sign-definite solitary waves, the VK stability criterion links the linear stability directly to the sign of the slope of the power curve [29,33]. For sign-indefinite gap solitons near band edges, we will show in the next section that this link also exists, but with important modifications depending on the sign of nonlinearity (i.e., focusing or defocusing). The power of the soliton (2.3) is defined as

$$P(\mu) = \langle u, u \rangle, \tag{2.30}$$

where the inner product is defined as

$$\langle f, g \rangle = \int_{-\infty}^{\infty} \int_{-\infty}^{\infty} f(x,y) g(x,y) dx dy. \tag{2.31}$$

Here the complex conjugate of f is not used since most variables involved in our inner products are real valued. For low-amplitude gap solitons near band edges, their power curve can be calculated asymptotically. By combining Eqs. (2.6), (2.8), and (2.22), the asymptotic expansion for the gap soliton is

$$u(x,y;X,Y) = \epsilon A(X,Y) p_1(x) p_2(y) + \epsilon^2 \left[\frac{\partial A}{\partial X} \nu_1(x) p_2(y) + \frac{\partial A}{\partial Y} p_1(x) \nu_2(y) \right] + O(\epsilon^3). \tag{2.32}$$

Substituting this expansion into Eq. (2.30), we get the power function $P(\mu)$ as

$$P(\mu) = P_0 + \epsilon P_1 + \epsilon^2 P_2 + \cdots, \tag{2.33}$$

where

$$P_0 = \epsilon^2 \int_{-\infty}^{+\infty} \int_{-\infty}^{+\infty} A^2(X,Y) p_1^2(x) p_2^2(y) dx dy, \tag{2.34}$$

$$P_1 = 2\epsilon^3 \int_{-\infty}^{+\infty} \int_{-\infty}^{+\infty} A(X,Y) p_1(x) p_2(y) \times \left[\frac{\partial A}{\partial X} \nu_1(x) p_2(y) + \frac{\partial A}{\partial Y} p_1(x) \nu_2(y) \right] dx dy, \tag{2.35}$$

and so on. The integrands of the above integrals are products between periodic Bloch functions in fast variables (x,y) and localized envelope functions in slow variables (X,Y). Using the formula in the Appendix, we find that the expressions of P_0 and P_1 for $\epsilon \ll 1$ are

$$P_0 = G \int_{-\infty}^{\infty} \int_{-\infty}^{\infty} A^2(X,Y) dX dY, \tag{2.36}$$

$$P_1 = 0, \tag{2.37}$$

where

$$G = \frac{1}{\pi^2} \int_0^{\pi} \int_0^{\pi} p_1^2(x) p_2^2(y) dx dy > 0 \tag{2.38}$$

is the average value of the squared Bloch-wave function $p_1^2(x) p_2^2(y)$. The errors in these expressions are exponentially small in ϵ, thus they do not affect the power series expansion (2.33) of the power function $P(\mu)$. Notice that the integral in Eq. (2.36) is the power of the envelope solution A in the 2D constant-coefficient NLS equation (2.24). By variable scalings, it is easy to find that

$$\int_{-\infty}^{\infty} \int_{-\infty}^{\infty} A^2(X,Y) dX dY = \frac{C_0 \sqrt{D_1 D_2}}{\alpha_0}, \tag{2.39}$$

where

$$C_0 = 11.70 \tag{2.40}$$

is the power of the ground-state soliton in the 2D NLS equation with unit dispersion and nonlinearity coefficients. Inserting this formula into Eq. (2.36), we get

$$P_0 = \frac{C_0 G \sqrt{D_1 D_2}}{\alpha_0}. \tag{2.41}$$

This P_0 is the limit power value of gap solitons on the edge of a Bloch band, and it is finite rather than infinite. Since $P_1 = 0$, then in view of $\mu - \mu_0 = O(\epsilon^2)$ out of Eq. (2.7), the power series expansion (2.33) gives

$$P(\mu) = P_0 + O(|\mu - \mu_0|), \tag{2.42}$$

which indicates that the power curve near a band edge is a linear function of μ.

It is noted that in the above asymptotic calculations of the power curves, the calculation results for the expansion coefficients P_n do not depend on whether the solitons are on site or off site. Indeed, the difference between on-site and off-site solitons is that the slow-variable functions [such as $A(X,Y)$] in the perturbative solutions $u_n(x,y,X,Y)$ are centered at different positions but have the same profiles, and these slow-variable functions are separated from the fast-variable functions. Thus when calculating the soliton's power, by using the integral formula of the Appendix, we see that the coefficients P_n would be the same for both on-site and off-site solitons. This means that near band edges, the power difference between on-site and off-site solitons is exponentially small in the soliton amplitude ϵ.

To compute the whole power curve of gap solitons both near and far away from band edges, the numerical methods need to be used. Here we use the modified squared-operator iteration method proposed in [41], which can converge to any gap soliton efficiently. The power curves of on-site solitons [see Figs. 1(a) and 1(d)] bifurcating from the two edges of the first Bloch band under focusing and defocusing nonlinearities are displayed in Fig. 2 (with $V_0 = 6$). We see that both power curves attain a minimum value inside the band gaps, and the shapes of these curves resemble the letter "v." In addition, these power curves increase as μ approaches band edges. These features of the power curves appear to be common for 2D gap solitons bifurcated from band edges (see [10] for further examples). Note that the powers of these gap

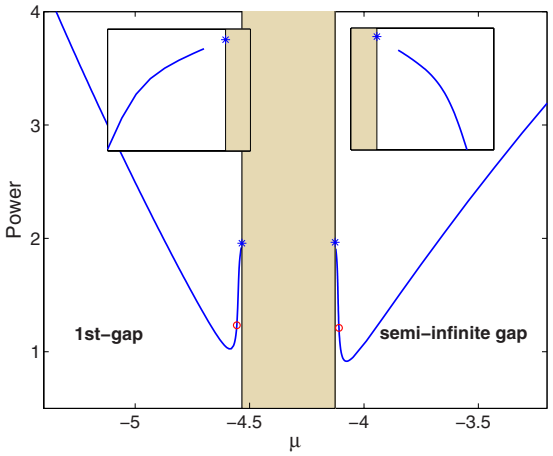

FIG. 2. (Color online) Power curves of on-site 2D gap solitons bifurcated from the first Bloch band under focusing and defocusing nonlinearities, respectively (V_0=6). The asterisks " *" are the analytical limit power values (2.41) at the band edges. The insets are enlargements of the power curves showing linear dependence near band edges. Soliton profiles at the right and left marked points (red circles) are displayed in the upper and lower rows of Fig. 1, respectively.

solitons are much less than the power C_0=11.70 of 2D solitons in Eq. (2.4) without the lattice potential. This means that these 2D gap solitons will not suffer the critical collapse of lattice-free 2D Kerr solitons [42]. The insets in Fig. 2 show that these power curves approach a straight line near the band edges, which agrees with the analytical results in Eq. (2.42). As μ approaches the right edge of the first band, the numerical power curve approaches a limit value P_0=1.9649, which agrees with the analytical formula (2.41). Similarly, as μ approaches the left edge of the first band, the numerical power curve approaches a limit value P_0=1.9567, which also agrees with the analytical formula (2.41).

III. LINEAR-INSTABILITY EIGENVALUES OF 2D GAP SOLITONS NEAR BAND EDGES

In this section, we study the linear stability of low-amplitude 2D gap solitons near band edges. These solitons are not sign definite in general (see Fig. 1), thus the VK stability criterion [29,33] does not apply to them. In addition to a zero eigenvalue, which is induced by the phase invariance of Eq. (2.1), these solitons also have three pairs of real or purely imaginary (nonzero) eigenvalues. The reason for this is that near band edges, gap solitons are governed by an envelope equation, which is the familiar 2D NLS equation with constant coefficients [see Eqs. (2.24) and (3.29) and [10]]. Solitons in this 2D envelope equation have a unique discrete eigenvalue, which is zero. Corresponding to this zero eigenvalue, there are four eigenfunctions. One is induced by the phase invariance of the envelope soliton, another two are induced by the translational invariance of the envelope soliton (along the two spatial dimensions), and the fourth one is induced by the variation of the envelope soliton with respect to its propagation constant. For gap solitons in the full model (2.1), the phase-invariance eigenmode of the envelope soliton persists, but the other three eigenmodes of the envelope soliton do not persist because the full model (2.1) is not translation invariant or its gap solitons do not have constant power. These three eigenmodes then have to bifurcate out from the zero eigenvalue. The bifurcated eigenvalues always appear as pairs of real or purely imaginary eigenvalues since the system is Hamiltonian. If the pair of eigenvalues bifurcating from the propagation-constant-variation eigenmode of the envelope soliton are unstable, they lead to width instabilities of gap solitons where the soliton width either steadily increases (the soliton decays) or decreases and relaxes into a periodic bound state (the soliton pulsates) depending on the initial power of the perturbed soliton [13,43]. If the two pairs of eigenvalues bifurcating from the translation-invariance eigenmodes of the envelope soliton are unstable, they lead to drift instabilities where the center of the soliton drifts away from its original location under perturbations. In this section, we focus on the pair of width-instability-type eigenvalues and derive their analytical expression near band edges by perturbation methods. This derivation does not depend on whether the gap solitons are on site or off site, thus our analytical formula is valid for both on-site and off-site solitons. This formula shows that one of this pair of eigenvalues is unstable if the slope of the power curve at the band edge has the opposite sign of nonlinearity σ, or equivalently, if the soliton's power near a band edge is lower than the limit power value on the band edge. Our computations of the power curves for a number of on-site and off-site gap-soliton branches in the model (2.4) show that this instability condition is always met under both focusing and defocusing cubic nonlinearities (see Figs. 2 and 3 for instance), thus these on-site and off-site 2D gap solitons near band edges are linearly unstable due to width instabilities. Extensions of this analysis to other spatial dimensions (such as 1D and 3D) will be discussed at the end of this section.

To study the linear stability of gap solitons $u(x,y)$, we perturb them in the normal-mode form as

$$U(x,y,t) = e^{i\mu t}\{u(x,y) + [v(x,y) - \lambda^{-1}w(x,y)]e^{i\lambda t} + [v^*(x,y) + \lambda^{*-1}w^*(x,y)]e^{-i\lambda^* t}\}, \quad (3.1)$$

where $v,w \ll 1$ are normal-mode perturbations, and the superscript * represents complex conjugation. Here we introduced a factor λ^{-1} in front of w, which gives the correct scaling of the normal-mode eigenfunction associated with the variation of the gap soliton with respect to its propagation constant for small eigenvalues λ. Substituting the perturbed solution (3.1) into the original evolution equation (2.1) and neglecting higher-order terms in (v,w), we obtain the standard eigenvalue problem

$$\mathcal{L}_1 v = w, \quad \mathcal{L}_0 w = \lambda^2 v, \quad (3.2)$$

where $\mathcal{L}_0$ has been defined in Eq. (2.10), and $\mathcal{L}_1$ is defined as

$$\mathcal{L}_1 = \frac{\partial^2}{\partial x^2} + \frac{\partial^2}{\partial y^2} - [F(x) + F(y)] - \mu + 3\sigma u^2(x,y). \quad (3.3)$$

Note that if (λ,v,w) is an eigenmode of Eq. (3.2), then so are $(-\lambda,v,w)$, (λ^*,v^*,w^*), and $(-\lambda^*,v^*,w^*)$ as well. Thus eigenvalues of Eq. (3.2) always appear in pairs or qua-

druples. In addition, we have the relation (2.11) as well as the relation

$$\mathcal{L}_1 u_\mu = u. \tag{3.4}$$

This second relation is obtained by taking the partial derivative of Eq. (2.11) with respect to μ. Furthermore, by taking the inner products of Eqs. (3.2) first equation with u_τ and the second equation with u, and recalling the self-adjoint properties of operators $(\mathcal{L}_0, \mathcal{L}_1)$ as well as the relations (2.11) and (3.4), we see that for nonzero eigenvalues λ, functions u and v are orthogonal to each other, and u_μ and w are orthogonal to each other, i.e.,

$$\langle u, v \rangle = 0, \tag{3.5}$$

and

$$\langle u_\mu, w \rangle = 0. \tag{3.6}$$

In our analysis below, we need to separate the partial derivatives in $\mathcal{L}_1$ into those with respect to the fast and slow variables as we have done for the operator $\mathcal{L}_0$. In doing so we get

$$\mathcal{L}_1 = M_0 + \epsilon M_1 + \epsilon^2 M_2 + 3\epsilon^2 \sigma (u_0 + \epsilon u_1 + \cdots)^2, \tag{3.7}$$

which is the analog of Eq. (2.12) for $\mathcal{L}_0$.

Our objective of this section is to determine the linear-stability eigenvalues λ and eigenfunctions (v, w) for low-amplitude 2D gap solitons near edges of Bloch bands. Before detailed calculations, we first lay out our plans. The eigenvalues of these gap solitons are clearly small since the soliton's amplitude is low. Then in view of Eqs. (2.11) and (3.2), we see that w should be proportional to u to the leading order. Indeed, we will find that $w \sim \epsilon u$ [see Eq. (3.50)]. Correspondingly, $v \sim \epsilon u_\mu$ in view of Eqs. (3.2) and (3.4). This eigenmode is associated with the soliton's variation with respect to the propagation constant μ. Indeed, we will show that this mode bifurcates from the eigenmode of the 2D envelope soliton's zero eigenvalue induced by this envelope soliton's variation with respect to its propagation constant [see Eq. (3.32)]. This mode leads to width instabilities of gap solitons when it is unstable, and to width oscillations of gap solitons when it is stable [13,43]. But w cannot be exactly equal to ϵu, because $w = \epsilon u$ cannot satisfy the orthogonality condition (3.6) in view that the power curve's slope is not zero near band edges (see Fig. 2). Calculation of the higher-order correction to the leading term ϵu of w is a key step in our analysis. Through systematic perturbative calculations, we will manage to show that the higher-order correction to w is given in Eq. (3.50), where the function ζ is given by Eq. (3.45) and is proportional to λ^2. Then by inserting this w formula into the orthogonality relation (3.6), the expression for the eigenvalue λ^2 will be obtained. It is noted that one can also determine the higher-order correction to the eigenfunction v and insert it into the orthogonality relation (3.5), which will produce the same expression for λ^2. But the former approach is a little simpler and thus will be adopted.

Now we start to calculate the power series expansions for the eigenmodes of low-amplitude gap solitons, which exist near band edges. For this purpose, we expand these eigenfunctions and the eigenvalue into the following power series of ϵ:

$$v = v_0 + \epsilon v_1 + \epsilon^2 v_2 + \cdots, \tag{3.8}$$

$$w = w_0 + \epsilon w_1 + \epsilon^2 w_2 + \cdots, \tag{3.9}$$

$$\lambda^2 = \epsilon \eta_1 + \epsilon^2 \eta_2 + \cdots. \tag{3.10}$$

Inserting these expansions and those of $\mathcal{L}_0$ and $\mathcal{L}_1$ into the eigenvalue problem (3.2), at $O(1)$ we get

$$M_0 w_0 = 0, \tag{3.11}$$

$$M_0 v_0 = w_0. \tag{3.12}$$

From Eq. (3.11), we see that $w_0 = h_0(X,Y) p_1(x) p_2(y)$. Due to the Fredholm condition for Eq. (3.12), one must have $h_0(X,Y) = 0$, thus $w_0 = 0$. Then from Eq. (3.12), we get

$$v_0 = \phi(X,Y) p_1(x) p_2(y). \tag{3.13}$$

At $O(\epsilon)$, we get

$$M_0 w_1 = \eta_1 v_0, \tag{3.14}$$

$$M_0 v_1 = w_1 - M_1 v_0. \tag{3.15}$$

Applying the Fredholm condition to Eq. (3.14), we see that $\eta_1 = 0$, hence $w_1 = h_1(X,Y) p_1(x) p_2(y)$. Applying the Fredholm condition to Eq. (3.15) and noticing that $M_1 v_0$ and $p_1(x) p_2(y)$ have the opposite symmetry in fast (x,y) variables and hence the integral of their product is zero over one period of $p_1(x)$ and $p_2(y)$, we find that $h_1(X,Y) = 0$, thus $w_1 = 0$. In this case, the solution v_1 is

$$v_1 = \frac{\partial \phi}{\partial X} \nu_1(x) p_2(y) + \frac{\partial \phi}{\partial Y} p_1(x) \nu_2(y). \tag{3.16}$$

Here we did not add Eq. (3.15)'s homogeneous solution of the form $h(X,Y) p_1(x) p_2(y)$ into v_1 because it turns out from later calculations that such a homogeneous term must be zero, thus we decided to leave it out at this early stage in order to simplify the analysis.

At $O(\epsilon^2)$, we get

$$M_0 w_2 = \eta_2 v_0, \tag{3.17}$$

$$M_0 v_2 = w_2 - M_1 v_1 - (M_2 + 3\sigma u_0^2) v_0. \tag{3.18}$$

Applying the Fredholm condition to Eq. (3.17), we get $\eta_2 = 0$. Thus

$$w_2 = \psi(X,Y) p_1(x) p_2(y). \tag{3.19}$$

The Fredholm condition for Eq. (3.18) is

$$\int_0^{2\pi} \int_0^{2\pi} [w_2 - M_1 v_1 - (M_2 + 3\sigma u_0^2) v_0] \times p_1(x) p_2(y) dx dy = 0. \tag{3.20}$$

Utilizing the expressions (3.13), (3.16), and (3.19) for

(v_0, v_1, w_2) as well as the relation (2.27), the above Fredholm condition reduces to

$$\mathcal{L}_1^e \phi = -\psi, \tag{3.21}$$

where

$$\mathcal{L}_1^e \equiv D_1 \frac{\partial^2}{\partial X^2} + D_2 \frac{\partial^2}{\partial Y^2} + \tau - 3\sigma\alpha_0 A^2. \tag{3.22}$$

Next we proceed to higher orders of ϵ. We will see that the equations for the next few higher-order terms in w are decoupled from the higher-order terms in v, thus we will consider higher-order terms in w only. At $O(\epsilon^3)$, we have

$$M_0 w_3 = \eta_3 v_0 - M_1 w_2. \tag{3.23}$$

Its Fredholm condition shows that $\eta_3 = 0$ [since the integral of $M_1 w_2$ multiplying $p_1(x)p_2(y)$ is zero over one period of $p_1(x)$ and $p_2(y)$]. In this case, the solution w_3 is then

$$w_3 = \frac{\partial \psi}{\partial X} \nu_1(x) p_2(y) + \frac{\partial \psi}{\partial Y} p_1(x) \nu_2(y). \tag{3.24}$$

Here we did not add Eq. (3.23)'s homogeneous solution of the form $h(X,Y)p_1(x)p_2(y)$ into w_3 either because such a term turns out to be zero as in the v_1 case.

At $O(\epsilon^4)$, we have

$$M_0 w_4 = \eta_4 v_0 - M_1 w_3 - (M_2 + \sigma u_0^2) w_2. \tag{3.25}$$

Its Fredholm condition gives

$$\int_0^{2\pi} \int_0^{2\pi} [\eta_4 v_0 - M_1 w_3 - (M_2 + \sigma u_0^2) w_2] \times p_1(x) p_2(y) dx dy = 0. \tag{3.26}$$

Utilizing the expressions (3.13), (3.19), and (3.24) for (v_0, w_2, w_3) as well as the relation (2.27), the above Fredholm condition reduces to

$$\mathcal{L}_0^e \psi = -\eta_4 \phi, \tag{3.27}$$

where

$$\mathcal{L}_0^e \equiv D_1 \frac{\partial^2}{\partial X^2} + D_2 \frac{\partial^2}{\partial X^2} + \tau - \sigma\alpha_0 A^2. \tag{3.28}$$

Now it is important to recognize that the two equations (3.21) and (3.27) form the eigenvalue problem for the linear stability of ground-state envelope solitons $Q(X,Y,T) = A(X,Y)e^{i\tau T}$ in the 2D envelope NLS equation [10]

$$iQ_Z - D_1 Q_{XX} - D_2 Q_{YY} + \sigma\alpha_0 |Q|^2 Q = 0. \tag{3.29}$$

The linear-stability spectrum of these ground-state solitons in this 2D constant-coefficient NLS equation is well known. It has a single discrete eigenvalue, which is zero. Thus $\eta_4 = 0$. Corresponding to this zero eigenvalue, there are three discrete eigenfunctions.

$$\phi = A_X, \quad \psi = 0, \tag{3.30}$$

$$\phi = A_Y, \quad \psi = 0, \tag{3.31}$$

and

$$\phi = A_\tau, \quad \psi = A. \tag{3.32}$$

The eigenfunctions (3.30) and (3.31) are induced by the translational invariance of the envelope soliton in the envelope equation (3.29), while the eigenfunction (3.32) is induced by the variation of this envelope soliton with respect to its propagation constant τ. It is noted that this envelope soliton also has a phase-invariance-induced eigenfunction at zero eigenvalue. But this phase-induced eigenmode does not satisfy the eigenvalue equations (3.21) and (3.27) of the envelope soliton, because these eigenvalue relations are obtained with the eigenfunction scalings as used in Eq. (3.1), which is not appropriate for the phase-induced eigenmode whose eigenvalue is always zero for both the envelope soliton and any gap soliton. Of the above eigenmodes of envelope solitons, we should point out that the propagation-constant-variation-induced eigenfunction (3.32) with eigenvalue zero only exists in two dimensions because 2D envelope solitons in Eq. (3.29) have constant powers for all propagation constants. This mode does not exist in other spatial dimensions (such as 1D or 3D) because powers of envelope solitons are not constant in such cases.

As we have mentioned earlier, the eigenvalues we will calculate in this section bifurcate from the eigenmode of the 2D envelope soliton's zero eigenvalue induced by this envelope soliton's variation with respect to its propagation constant, thus we will take Eq. (3.32) for the following analysis. In this case, by comparing the expressions (3.13), (3.16), and (3.19), and (3.24) for (v_0, v_1, w_2, w_3) with the expressions (2.8) and (2.22) for (u_0, u_1), we see that

$$v_0 = u_{0\tau}, \quad v_1 = u_{1\tau}, \tag{3.33}$$

$$w_0 = w_1 = 0, \quad w_2 = u_0, \quad w_3 = u_1. \tag{3.34}$$

In addition,

$$\eta_1 = \eta_2 = \eta_3 = \eta_4 = 0. \tag{3.35}$$

Next we continue to pursue higher-order terms in the power series expansions of the eigenfunction w and eigenvalue λ^2. The function w_4 satisfies Eq. (3.25). Utilizing Eqs. (2.18), (3.34), and (3.35), we find that

$$w_4 = u_2 + \zeta(X,Y) p_1(x) p_2(y). \tag{3.36}$$

Here the inclusion of the homogeneous solution $\zeta(X,Y)p_1(x)p_2(y)$ in w_4 is necessary, and in fact crucial, in our analysis. To obtain the equation for w_5, we expand the eigenvalue problem (3.2) to $O(\epsilon^5)$ and get

$$M_0 w_5 = \eta_5 v_0 - M_1 w_4 - (M_2 + \sigma u_0^2) w_3 - 2\sigma u_0 u_1 w_2. \tag{3.37}$$

Inserting the expressions (3.13), (3.34), and (3.36) for (v_0, w_2, w_3, w_4) into the above equation and utilizing the Fredholm condition on the u_3 equation (2.19), one can readily show that the Fredholm condition for Eq. (3.37) is satisfied only when $\eta_5 = 0$. In this case, by utilizing the u_3 equation (2.19), the solution w_5 can be found to be

$$w_5 = u_3 + \frac{\partial \zeta}{\partial X} v_1(x) p_2(y) + \frac{\partial \zeta}{\partial Y} p_1(x) v_2(y) + \gamma(X,Y) p_1(x) p_2(y). \tag{3.38}$$

Here the γ term will not enter the leading-order asymptotic expression of the eigenvalues, and thus does not need much attention.

Next we proceed to the equation for w_6, whose Fredholm condition will determine the function $\zeta(X,Y)$ in the expression (3.36) of w_4. The equation for w_6 can be obtained by expanding the eigenvalue problem (3.2) to $O(\epsilon^6)$, and we get

$$M_0 w_6 = \eta_6 v_0 - M_1 w_5 - (M_2 + \sigma u_0^2) w_4 - 2\sigma u_0 u_1 w_3 - \sigma(2u_0 u_2 + u_1^2) w_2. \tag{3.39}$$

Its Fredholm condition is

$$\int_0^{2\pi} \int_0^{2\pi} [\eta_6 v_0 - M_1 w_5 - (M_2 + \sigma u_0^2) w_4 - 2\sigma u_0 u_1 w_3 - \sigma(2u_0 u_2 + u_1^2) w_2] p_1(x) p_2(y) dx dy = 0. \tag{3.40}$$

Inserting the expressions (3.13), (3.34), (3.36), and (3.38) of $(v_0, w_2, w_3, w_4, w_5)$ into the above condition and utilizing the Fredholm condition on the u_4 equation (2.20) as well as the relation (2.27), we find that the above Fredholm condition (3.40) reduces to

$$\mathcal{L}_0^e \zeta = -\eta_6 A_\tau. \tag{3.41}$$

This equation determines the function ζ. Notice that A satisfies Eq. (2.24), i.e., $\mathcal{L}_0^e A = 0$, thus Eq. (3.41) has a homogeneous solution A. This homogeneous solution is orthogonal to the inhomogeneous term A_τ since the power of envelope solitons A in Eq. (2.24) is independent of the parameter τ. Thus Eq. (3.41) admits a localized solution ζ. This ζ solution is not unique because $\zeta + \alpha A$ is also a solution of Eq. (3.41) for any constant α. Recalling Eqs. (2.8), (3.34), and (3.36), we see that the homogeneous term αA in the ζ solution leads to a scaling of the eigenfunction w from w to $(1+\epsilon^2\alpha)w$, which does not affect the eigenvalue at all. This can be further confirmed by Eqs. (3.53)–(3.59), where it is seen that any homogeneous term αA in ζ has zero contribution to the eigenvalue formula.

The solution ζ of Eq. (3.41) can be derived more explicitly as follows. By differentiating Eq. (2.24) with respect to τ, we find that

$$\mathcal{L}_1^e A_\tau = -A. \tag{3.42}$$

When this relation is combined with Eq. (3.41), we get

$$\mathcal{L}_1^e \mathcal{L}_0^e \zeta = \eta_6 A. \tag{3.43}$$

By introducing normalized variables

$$\bar{X} = \left|\frac{\tau}{D_1}\right|^{1/2} X, \quad \bar{Y} = \left|\frac{\tau}{D_2}\right|^{1/2} Y, \quad \bar{A} = \left|\frac{\alpha_0}{\tau}\right|^{1/2} A \tag{3.44}$$

to the above equation and noticing the conditions (2.28) on the signs of D_1, D_2, τ, and σ for solitary waves in the envelope equation (2.24), we find that the function ζ can be expressed as

$$\zeta = \frac{\eta_6}{|\tau|\sqrt{\alpha_0|\tau|}} \bar{\zeta}(\bar{X}, \bar{Y}), \tag{3.45}$$

where $\bar{\zeta}(\bar{X}, \bar{Y})$ is a symmetric solution of the following parameter-free equation:

$$\bar{\mathcal{L}}_1 \bar{\mathcal{L}}_0 \bar{\zeta}(\bar{X}, \bar{Y}) = \bar{A}. \tag{3.46}$$

Here $\bar{A}(\bar{X}, \bar{Y})$ is the unique ground-state solution of the following parameter-free 2D NLS equation

$$\bar{\mathcal{L}}_0 \bar{A}(\bar{X}, \bar{Y}) = 0, \tag{3.47}$$

and $\bar{\mathcal{L}}_0, \bar{\mathcal{L}}_1$ are the normalized linear operators

$$\bar{\mathcal{L}}_0 \equiv \frac{\partial^2}{\partial \bar{X}^2} + \frac{\partial^2}{\partial \bar{Y}^2} - 1 + \bar{A}^2, \tag{3.48}$$

$$\bar{\mathcal{L}}_1 \equiv \frac{\partial^2}{\partial \bar{X}^2} + \frac{\partial^2}{\partial \bar{Y}^2} - 1 + 3\bar{A}^2. \tag{3.49}$$

To summarize the above results, we insert the expressions (3.34) and (3.36) for (w_2, w_3, w_4) into the perturbation series expansion (3.9), and find that the asymptotic formula for the eigenfunction w is

$$w = \epsilon[u + \epsilon^3 \zeta(X,Y) p_1(x) p_2(y) + O(\epsilon^4)], \tag{3.50}$$

where ζ is given by Eq. (3.45). The reader is reminded here that the leading-order term of u is $O(\epsilon)$ [see Eq. (2.6)].

Now we insert the above perturbation-series solution of w into the orthogonality relation (3.6). To leading orders, we get

$$\langle u_\mu, u + \epsilon^3 \zeta(X,Y) p_1(x) p_2(y) \rangle = 0. \tag{3.51}$$

Notice that

$$\langle u_\mu, u \rangle = \frac{1}{2} P'(\mu), \tag{3.52}$$

where P is the power of the soliton defined in Eq. (2.30). By taking the leading-order term ϵu_0 of u and using the relation (2.7) between μ and τ, we find that to the leading order,

$$\langle u_\mu, \epsilon^3 \zeta(X,Y) p_1(x) p_2(y) \rangle = \epsilon^2 \langle A_\tau(X,Y) p_1(x) p_2(y), \zeta(X,Y) p_1(x) p_2(y) \rangle. \tag{3.53}$$

Using the integral formula in the Appendix, the above equation becomes

$$\langle u_\mu, \epsilon^3 \zeta(X,Y) p_1(x) p_2(y) \rangle = G \int_{-\infty}^{\infty} \int_{-\infty}^{\infty} A_\tau(X,Y) \zeta(X,Y) dX dY, \tag{3.54}$$

where G is the average value of the squared Bloch-wave function $p_1^2(x) p_2^2(y)$ as defined in Eq. (2.38). To evaluate the integral in the right-hand side of the above equation, we see from Eq. (3.41) and Eqs. (3.44)–(3.46) that

$$A_\tau = \frac{\sigma}{\sqrt{\alpha_0|\tau|}} \bar{\mathcal{L}}_1^{-1} \bar{A}(\bar{X},\bar{Y}). \tag{3.55}$$

Then using the normalized variables (3.44) as well as the above expression (3.55) for A_τ and expression (3.45) for ζ, one finds that

$$\int_{-\infty}^{\infty}\int_{-\infty}^{\infty} A_\tau(X,Y)\zeta(X,Y)dXdY = -\frac{\eta_6 C_1\sqrt{D_1 D_2}}{\alpha_0\tau^3}, \tag{3.56}$$

where

$$C_1 \equiv -\int_{-\infty}^{\infty}\int_{-\infty}^{\infty} \bar{\zeta}(\bar{X},\bar{Y})\bar{\mathcal{L}}_1^{-1}\bar{A}(\bar{X},\bar{Y})d\bar{X}d\bar{Y} = 0.8684. \tag{3.57}$$

Inserting the expressions (3.52), (3.54), and (3.56) into Eq. (3.51), we obtain the coefficient η_6 as

$$\eta_6 = \frac{P'(\mu_0)\alpha_0\tau^3}{2C_1 G\sqrt{D_1 D_2}}. \tag{3.58}$$

Substituting this expression into the expansion (3.10) of λ^2 and recalling the relation (2.7) as well as the power formula (2.41), we finally obtain the leading-order asymptotic expression for λ^2 as

$$\lambda^2 = \frac{C_0}{2C_1}\frac{P'(\mu_0)}{P(\mu_0)}(\mu-\mu_0)^3, \tag{3.59}$$

where $P(\mu_0)=P_0$ is the limit power value at the band edge μ_0 [see Eq. (2.41)], and constants (C_0, C_1) are given in Eqs. (2.40) and (3.57). This asymptotic formula is the most important result of this paper. It has far-reaching consequences, which we will elaborate on below.

First this formula shows that λ^2 is always real. If λ^2 is positive, then λ is real and stable, while if λ^2 is negative, then λ is purely imaginary and unstable. In view of Eqs. (2.7) and (2.28), we see that $\mathrm{sgn}(\mu-\mu_0)=\mathrm{sgn}(\sigma)$, thus the formula (3.59) also shows that

$$\mathrm{sgn}(\lambda^2) = \mathrm{sgn}[\sigma P'(\mu_0)]. \tag{3.60}$$

This relation tells us that for the focusing nonlinearity (where $\sigma=1$), the eigenvalue λ is unstable if $P'(\mu_0)$ is negative, i.e., if the slope of the power curve at the band edge is negative. This is analogous to the VK stability criterion (although the gap soliton here is sign indefinite in general). But *for the defocusing nonlinearity* (*where* $\sigma=-1$), *this eigenvalue is unstable if* $P'(\mu_0)$ *is positive.* This is just the opposite of what the VK criterion says. These results generalize and modify the VK stability criterion to sign-indefinite gap solitons, and reveal the important role the sign of nonlinearity plays in the connection between stability and the power slope.

The above conditions for linear instability can be combined into one equivalent but simpler condition. Notice that under focusing nonlinearity, gap solitons bifurcate out at the right-hand side of a band edge. Thus when $P'(\mu_0)<0$, the powers of gap solitons near the band edge are lower than the limit power value P_0 at the band edge. Under defocusing nonlinearity, gap solitons bifurcate out at the left-hand side of a band edge. Thus when $P'(\mu_0)>0$, the powers of gap solitons near the band edge are also lower than the limit power value P_0 at the band edge. As a result, our results above for linear instability of gap solitons for both focusing and defocusing nonliearities can be condensed into the following simple statement: *gap solitons near band edges are unstable if their powers are lower than the limit power values on the band edges.*

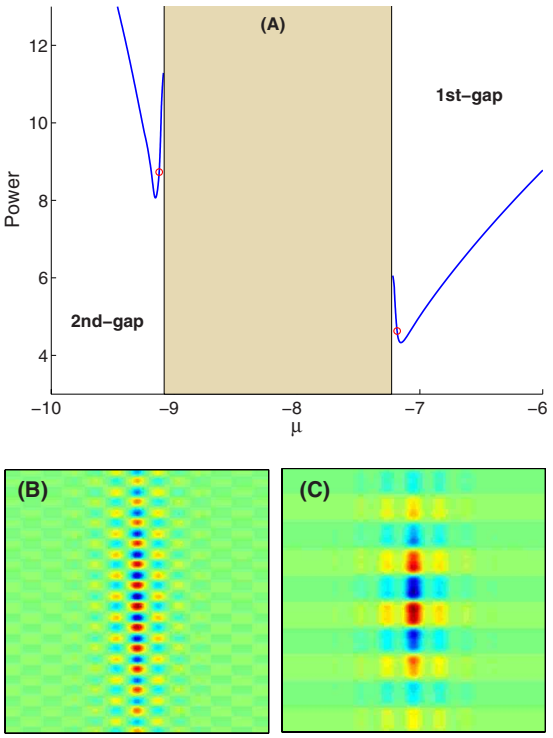

FIG. 3. (Color online) (A) Power curves of on-site single-Bloch-wave gap solitons bifurcated from the right and left edges of the second Bloch band under focusing and defocusing nonlinearities, respectively ($V_0=6$). [(B) and (C)] Profiles of gap solitons at the left and right red circles of the power curves in (A).

Formula (3.59) also tells us that the eigenvalue λ is proportional to $|\mu-\mu_0|^{3/2}$. Recalling Eq. (2.7), we see that $|\mu-\mu_0|^{3/2}$ is proportional to ϵ^3, where ϵ is the amplitude of the gap soliton. Thus the eigenvalue λ is proportional to the cubic power of the soliton's amplitude.

Now we check if the above instability condition on the power curve is satisfied or not for 2D gap solitons. First we examine the on-site gap solitons near the left and right edges of the first Bloch band, whose power curves have been plotted in Fig. 2. A quick inspection of this figure shows that for both families of gap solitons, their powers near band edges are lower than the limit powers on the band edges, thus these solitons near band edges are linearly unstable. In order to check if this instability condition is satisfied for other branches of gap solitons, we consider the on-site single-Bloch-wave gap solitons near the left and right edges of the second Bloch band for the defocusing and focusing nonlinearities ($V_0=6$). The power curves of these solitons are plotted in Fig. 3(a), and typical soliton profiles near band edges are displayed in Figs. 3(b) and 3(c). These solitons are very

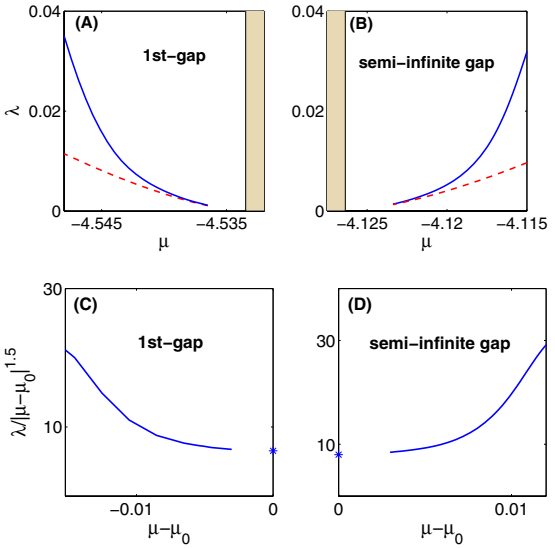

FIG. 4. (Color online) [(A) and (B)] Unstable eigenvalues of on-site gap solitons near the left and right edges of the first Bloch band in Fig. 2. Solid lines: numerical results; dashed lines: analytical formulas (3.61). The shaded regions represent the first Bloch band. [(C) and (D)] Curves of $|\lambda/(\mu-\mu_0)^{3/2}|$ vs $\mu-\mu_0$ for the two branches of unstable eigenvalues in (A) and (B). * represents the theoretical β value from Eq. (3.61).

broad along one direction and very narrow along the orthogonal direction, and they have been called reduced-symmetry solitons in [19] (see also [10]). Here again, the instability condition is satisfied for both branches of gap solitons, thus these solitons near band edges [such as those displayed in Figs. 3(b) and 3(c)] are linearly unstable as well. For off-site gap solitons near these band edges of Figs. 2 and 3, since their power curves are asymptotically the same as those of on-site solitons (see discussions near the end of the previous section), we conclude that off-site gap solitons near these band edges are linearly unstable as well.

The above analytical prediction of unstable eigenvalues for gap solitons near band edges is fully confirmed both qualitatively and quantitatively by our direct numerical computations. For gap solitons near band edges, the unstable eigenvalues are very small. In order to accurately determine these small eigenvalues, several well known methods [such as simulating the linearized wave equation of Eq. (2.1) to pick up its exponential growth or discretizing the operator eigenvalue problem (3.2) into a matrix eigenvalue problem] are inefficient. Here we use our newly developed iteration method, which can obtain small eigenvalues efficiently and accurately [44]. With this method, we indeed found unstable eigenvalues for gap solitons of Figs. 2 and 3 near band edges, confirming the qualitative analytical predictions above. To make quantitative comparisons, we consider the two branches of on-site gap solitons near edges of the first Bloch band under focusing and defocusing nonlinearities, which are displayed in Figs. 1(a), 1(d), and 2. The numerically obtained unstable eigenvalues for these gap solitons are plotted in Figs. 4(a) and 4(b) (solid lines). To compare with the asymptotic formula (3.59), we first rewrite Eq. (3.59) as

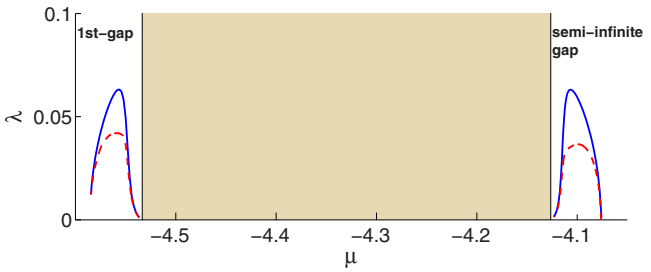

FIG. 5. (Color online) Whole curves of unstable eigenvalues for the two branches of on-site gap solitons in Fig. 2. Solid lines: numerical results; dashed lines: modified analytical formula (3.62).

$$\lambda = \pm i\beta|\mu-\mu_0|^{3/2}, \quad \beta \equiv \left[\frac{C_0}{2C_1}\frac{|P'(\mu_0)|}{P(\mu_0)}\right]^{1/2}. \tag{3.61}$$

From Fig. 2, we see that for solitons in the semi-infinite gap, $P(\mu_0)=1.9649$ and $P'(\mu_0)=-18.6414$, thus the coefficient $\beta=7.9942$, while for solitons in the first gap, $P(\mu_0)=1.9567$ and $P'(\mu_0)=12.4885$, thus $\beta=6.5572$. Inserting these values into the asymptotic formula (3.61), these leading-order analytical results are also plotted in Figs. 4(a) and 4(b) (dashed lines) for comparison. As we can see, the numerical curves approach the analytical ones as μ approaches the band edges, confirming the asymptotic formula (3.61). A more accurate way to confirm the formula (3.61) is to plot the function $|\lambda/(\mu-\mu_0)^{3/2}|$ against $\mu-\mu_0$ from the numerical data. According to the asymptotic formula (3.61), $|\lambda/(\mu-\mu_0)^{3/2}|$ should approach the constant β as μ approaches the band edge μ_0. To verify this, we have taken the numerically obtained unstable eigenvalues and plotted the functions $|\lambda/(\mu-\mu_0)^{3/2}|$ in Figs. 4(c) and 4(d). The theoretical β values from Eq. (3.61) are also shown by the asterisk symbols. It is seen that at both band edges, the functions $|\lambda/(\mu-\mu_0)^{3/2}|$ indeed approach the theoretical β values as μ approaches the band edges. This agreement unambiguously confirms the asymptotic formula (3.61) and its equivalent form (3.59).

Away from band edges, the leading-order asymptotic formula (3.59) will become less accurate. In such cases, the numerical method of [44] can be utilized to obtain the whole curve of unstable eigenvalues. For the two branches of on-site gap solitons shown in Fig. 2, these whole curves of unstable eigenvalues are plotted in Fig. 5. The most important feature of these two curves is that these eigenvalues are only unstable near the band edges, but become stable some distance away from the band edges. This makes the unstable-eigenvalue curve to be shaped roughly like the letter "n." The location where this eigenvalue changes from unstable to stable is precisely where the slope of the power curve is zero, i.e., where the power attains its minimum value. This exchange of stability at the minimum power point is already indicated by the VK stability criterion for sign-definite gap solitons. For sign-indefinite gap solitons where the VK criterion does not apply, one can still show by other methods (such as the asymptotic method) that a width-instability-related eigenvalue changes from unstable to stable at every

power extremum point, which explains our numerical results in Fig. 5. If one wants to obtain an analytical formula which can well approximate the entire n-shaped eigenvalue curve of Fig. 5, he would need to calculate higher-order corrections to the leading-order eigenvalue formula (3.59), which will be expensive to do. Below, motivated by the form of the asymptotic formula (3.59) as well as the fact of exchange of stability at a power extremum point, we propose an approximate eigenvalue formula for the whole range of μ values as

$$\lambda^2 = \frac{C_0}{2C_1}\frac{P'(\mu)}{P(\mu)}(\mu - \mu_0)^3. \tag{3.62}$$

Here instead of using the power and its slope values at the band edge μ_0, we use such values at the local point μ where the eigenvalue is calculated. This modified eigenvalue formula has two main properties. One property is that near a band edge μ_0, this new formula asymptotically approaches the previous formula (3.59). The other property is that at a power extremum point, the eigenvalue of this modified formula changes from unstable to stable, which qualitatively agrees with the fact mentioned above. Due to these two properties, this modified formula would give quantitatively accurate eigenvalues near band edges and qualitatively accurate eigenvalues away from band edges. To compare this modified eigenvalue formula with the numerical values, we use the power curves of Fig. 2, which enable us to calculate these modified eigenvalues. The results are displayed in Fig. 5 as dashed lines. When compared to the numerically obtained eigenvalues (solid lines), we find that this modified formula gives a decent approximation for the unstable eigenvalues over the whole range of the μ intervals.

We emphasize that the above asymptotic eigenvalue formula (3.59) holds identically for both on-site and off-site gap solitons near band edges. Indeed, in all our calculations of power series expansions, we did not use any information on the center locations of gap solitons. This means that the difference in eigenvalues between on-site and off-site solitons near band edges is smaller than any power of the soliton amplitude ϵ, i.e., is exponentially small in ϵ.

As we have mentioned earlier in this section, the eigenvalues calculated above bifurcate from the eigenmode (3.32) of the 2D envelope soliton's zero eigenvalue induced by this envelope soliton's variation with respect to its propagation constant. These eigenvalues, if unstable, lead to width instabilities. We should point out that gap solitons also possess other eigenvalues, which bifurcate from the eigenmodes (3.30) and (3.31) of the envelope soliton's zero eigenvalue induced by this envelope soliton's variation with respect to its spatial positions. These eigenvalues, if unstable, lead to drift instabilities. In one dimension, it has been shown that for gap solitons near band edges, these position-variation-induced eigenvalues are exponentially small with the soliton's amplitude. In addition, these eigenvalues are stable for on-site solitons but unstable for off-site solitons [25]. In the 2D case, similar results hold, i.e., these position-variation-induced eigenvalues are also exponentially small, and they are stable for on-site solitons but unstable for off-site solitons (details omitted). Physically speaking, the centers of off-site solitons are at a local maximum of the lattice potential $V(x,y)$, thus they are unstable, and their centers tend to drift from a potential maximum (off site) to a potential minimum (on site). In two dimensions, since we have shown that both on-site and off-site gap solitons suffer width instabilities near band edges (based on the power curves we have obtained, see Figs. 2 and 3), the presence or absence of these drift instabilities will not change the unstable nature of gap solitons near band edges.

In the above analysis, we have established both analytically and numerically that 2D gap solitons near band edges are linearly unstable. Then how will these unstable solitons evolve under perturbations? Here we briefly address this question. For on-site 2D gap solitons, the instability is only the width-instability type, and drift instabilities are absent. The nonlinear evolution of such on-site solitons under perturbations has been illustrated in [13]. If the initial perturbation reduces the power of the soliton, the soliton will decay, and its width will steadily increase. But if the initial perturbation increases the power of the soliton, the soliton will shrink into a narrower but higher hump. These two scenarios can be heuristically understood from the envelope dynamics of these gap solitons, which are governed by the 2D NLS equation (3.29). It is well known that in this 2D NLS equation for the Bloch-wave envelope, if the initial condition is a reduced (envelope) soliton, then the solution will disperse away; but if the initial condition is an amplified soliton (so that the energy of the initial state is negative), then the solution will become singular in finite time (critical collapse) [42]. This envelope dynamics in the 2D NLS equation explains the gap-soliton dynamics near band edges under perturbations (during the initial stage of evolution). In the second case where the gap soliton shrinks and steepens (corresponding to critical collapse in the envelope of the gap soliton), since the total power of the gap soliton is less than the critical power (i.e., $C_0=11.70$) of lattice-free Kerr solitons (see Figs. 2 and 3), critical collapse in the lattice model (2.1) cannot happen [42]. Thus this steepened solution has to retreat and evolve into an oscillating bound state where the solution pulsates. This behavior is qualitatively similar to that in a 1D model under dual-power-law nonlinearities [43].

For off-site gap solitons, however, the drift instabilities are also present. Due to both the width and drift instabilities, a perturbed off-site soliton will generally drift to a lattice site (in an oscillatory manner). At the same time, it will decay away or relax into a pulsating bound state.

In the end of this section, we examine the implications of our 2D stability analysis for other spatial dimensions. For low-amplitude gap solitons near band edges, their linear-stability eigenvalues bifurcate from eigenmodes of the envelope soliton in the envelope equation. In the 1D case, the envelope soliton in the envelope equation (i.e., 1D NLS equation) has a single discrete eigenvalue, which is zero. At this zero eigenvalue, there are only two discrete eigenfunctions, which are induced by the phase and position invariances of the envelope soliton. There does not exist the propagation-constant-variation-type eigenmode [the counterpart of Eq. (3.32)], thus the eigenvalues (3.59) we calculated for 2D gap solitons have no counterpart in 1D gap solitons. In the 3D case (i.e., "light bullet" gap solitons trapped in a 3D lattice and evolving with time), the envelope soliton in

the envelope equation (i.e., 3D NLS equation) has a zero discrete eigenvalue and a pair of nonzero discrete eigenvalues (one of which is unstable). This zero eigenvalue contains four eigenfunctions (three induced by position invariance, and one by phase invariance), and these eigenmodes are not related to the eigenvalues calculated in this paper. But the nonzero eigenvalues of 3D envelope solitons are directly related to our stability analysis, and their bifurcations in 3D gap solitons near band edges can be readily derived from our existing formulas. Indeed, the counterpart of the envelope soliton's eigenvalue problem (3.21) and Eq. (3.27) in 3D has a negative eigenvalue η_4, thus one gets from Eq. (3.10) that to leading order, $\lambda^2=\eta_4\epsilon^4$, thus $\lambda=\pm i\sqrt{|\eta_4|}\epsilon^2$. One of this pair of eigenvalues is unstable, thus low-amplitude 3D gap solitons near band edges are always linearly unstable. This linear instability of the 3D gap solitons is directly caused by the linear instability of 3D envelope solitons (comparatively, 2D envelope solitons are linearly neutrally stable and nonlinearly unstable [42]). The magnitude of this unstable eigenvalue of 3D gap solitons is proportional to the square of the soliton's amplitude, which is larger than that of 2D gap solitons.

IV. SUMMARY AND DISCUSSIONS

In this paper, linear stability properties of 2D low-amplitude single-Bloch-wave packet gap solitons near edges of Bloch bands in a cubic nonlinear medium has been determined both analytically and numerically. Through asymptotic analysis, it has been shown that these gap solitons are linearly unstable if the slope of their power curve at the band edge has the opposite sign of the nonlinearity. This generalizes and modifies the VK stability criterion to sign-indefinite gap solitons under either focusing or defocusing nonlinearities. Through numerical computations of the power curves near several band edges, it has been found that this condition is always satisfied, thus 2D gap solitons near band edges are linearly unstable (for both focusing and defocusing nonlinearities). The analytical formula for this unstable eigenvalue of gap solitons near band edges has also been asymptotically derived. It is shown that this eigenvalue is proportional to the cubic power of the soliton's amplitude, and it induces width instabilities of gap solitons. Comparison between this eigenvalue formula and numerically computed eigenvalues shows excellent agreement.

We should emphasize that our instability results were derived for 2D gap solitons near band edges where the soliton amplitudes are small. Away from band edges (i.e., at higher soliton amplitudes), while off-site solitons will remain unstable since the drift instabilities will persist, on-site solitons, however, can become stable. The reason for this stability is that the width-instability eigenvalue will become stable when the propagation constant crosses over a power minimum point. This is illustrated clearly in Fig. 5 (see also [13]). Thus high-amplitude on-site 2D gap solitons in a cubic nonlinear medium can be stable and physically observable. In a saturable photorefractive medium, such solitons in the semi-infinite and first band gaps under both focusing and defocusing nonlinearities have been observed in [5,6,17,19].

The results of this paper shed much light on stability properties of 2D gap solitons in a cubic nonlinear medium, but some important questions still remain open. One question is what will happen if the nonlinearity is not cubic but rather saturable. This question is significant because many recent optical experiments on periodic media were performed in photorefractive crystals whose nonlinearity is saturable [5,36]. Under the saturable nonlinearity, will the stability properties of 2D gap solitons near band edges remain the same as those for the cubic nonlinearity? Note that according to the numerical results of [45], powers of 2D gap solitons on the band edges can be lower than those near band edges under defocusing saturable nonlinearity (see their Fig. 6). Based on our stability results for cubic nonlinearities, this could suggest that such gap solitons near band edges are linearly stable. Motivated by this prospect, we redid their power calculations in Fig. 6 using the recently developed modified squared operator iteration method [41]. Our results show that, different from their findings, the power of those 2D gap solitons on the band edge is still higher than that near the band edge, similar to the cubic-nonlinearity case. Thus we conjecture that low-amplitude 2D gap solitons near band edges in the saturable model are linearly unstable as well—a conjecture which needs substantiation. Another open question is the following. In this paper, we only considered the stability of 2D gap solitons in the form of single-Bloch-wave packets. But it is known that near many 2D band edges, gap solitons consisting of two coupled Bloch-wave packets exist [10]. Examples include the dipole-array solitons and vortex-array solitons near band edges "*C*" and "*D*" in [10]. Stability properties of such coupled Bloch-wave packet solitons are still unknown. These open questions lie outside the scope of the present paper, but they certainly merit further studies in the future.

Lastly, we would like to point out that the results of this paper have direct ramifications to other areas of nonlinear wave dynamics. For instance, in the theory of nonlinear water waves, it was shown recently that two-dimensional wave-packet solutions (lumps) can bifurcate from the edge of the continuous spectrum in the fifth-order Kadomtsev-Petviashivili (KP) equation [46]. The power curve of these lumps has a v shape, and the lumps near the edge of the continuous spectrum are linearly unstable [46]. These phenomena closely resemble those of 2D gap solitons in the model equation (2.1). Clearly our stability analysis can be extended to lumps in the fifth-order KP equation, and an eigenvalue formula similar to Eq. (3.59) can be derived (except that the constants C_0 and C_1 are now different).

ACKNOWLEDGMENTS

This work was partially supported by the Air Force Office of Scientific Research and the National Science Foundation.

APPENDIX: AN EXPONENTIALLY ACCURATE INTEGRAL FORMULA

In the analysis of this paper, we often needed to calculate integrals of functions, which are products between a slow-

variable localized function and a fast-variable periodic function. To calculate such integrals, the following asymptotic formulas have been used. These asymptotic formulas are exponentially accurate, thus they do not affect the power series expansions in our analysis.

If $f(x)$ is a T-periodic function, $X=\epsilon x$ is a slow variable with $\epsilon \ll 1$, and $F(X)$ is a smooth localized function of X, then the following asymptotic formula holds:

$$\int_{-\infty}^{\infty} f(x)F(X)dx = \frac{G}{\epsilon}\int_{-\infty}^{\infty} F(X)dX + o(\epsilon^n), \tag{A1}$$

where

$$G \equiv \frac{1}{T}\int_0^T f(x)dx \tag{A2}$$

is the average value of the periodic function $f(x)$, and n is any integer. The arbitrariness of n indicates that the error in the asymptotic approximation (A1) is exponentially small in ϵ.

The above formula can be easily proved as the following. We first expand the periodic function $f(x)$ into the Fourier series as follows:

$$f(x) = \sum_{n=-\infty}^{\infty} c_n e^{i2\pi nx/T}. \tag{A3}$$

Substituting this expansion into the left-hand side of Eq. (A1), we get

$$\int_{-\infty}^{\infty} f(x)F(X)dx = c_0\int_{-\infty}^{\infty} F(X)dx + \sum_{n\neq 0} c_n \int_{-\infty}^{\infty} F(X)e^{i2\pi nx/T}dx. \tag{A4}$$

Notice that

$$c_0 = \frac{1}{T}\int_0^T f(x)dx = G, \tag{A5}$$

thus the first term in (A4) is equal to the first term in the formula (A1). Regarding the remaining terms in Eq. (A4), we see that

$$\int_{-\infty}^{\infty} F(X)e^{i2\pi nx/T}dx = \frac{1}{\epsilon}\int_{-\infty}^{\infty} F(X)e^{i2\pi nX/\epsilon T}dX = \frac{1}{\epsilon}\mathcal{F}\left(-\frac{n}{\epsilon T}\right), \tag{A6}$$

where $\mathcal{F}(\cdot)$ is the Fourier transform of $F(X)$. If $F(X)$ is a smooth function and $n\neq 0$, it is well known that the Fourier coefficient $\mathcal{F}$ at large wave number $-n/\epsilon T$ is smaller than any power of ϵ. Thus formula (A1) is proved.

The 1D formula (A1) is simple to extend to higher dimensions. The 2D counterpart of this formula is

$$\int_{-\infty}^{\infty}\int_{-\infty}^{\infty} f(x,y)F(X,Y)dxdy = \frac{G}{\epsilon^2}\int_{-\infty}^{\infty}\int_{-\infty}^{\infty} F(X,Y)dXdY + o(\epsilon^n). \tag{A7}$$

Here $f(x,y)$ is a T-periodic function in both x and y, $X=\epsilon x, Y=\epsilon y$ are slow variables, $F(X,Y)$ is a smooth localized function of (X,Y), and G is the average value of the periodic function $f(x,y)$.

$$G \equiv \frac{1}{T^2}\int_0^T\int_0^T f(x,y)dxdy. \tag{A8}$$

[1] P. Russell, Science **299**, 358 (2003).
[2] H. S. Eisenberg, Y. Silberberg, R. Morandotti, A. R. Boyd, and J. S. Aitchison, Phys. Rev. Lett. **81**, 3383 (1998).
[3] T. Liu, M. Fallahi, J. V. Moloney, and M. Mansuripur, IEEE Photonics Technol. Lett. **18**, 1100 (2006).
[4] A. Szameit, J. Burghoff, T. Pertsch, S. Nolte, A. Tnnermann, and F. Lederer, Opt. Express **14**, 6055 (2006).
[5] J. W. Fleischer, M. Segev, N. K. Efremidis, and D. N. Christodoulides, Nature (London) **422**, 147 (2003).
[6] H. Martin, E. D. Eugenieva, Z. Chen, and D. N. Christodoulides, Phys. Rev. Lett. **92**, 123902 (2004).
[7] Z. Chen and J. Yang, *Nonlinear Optics and Applications* (Research Signpost, Kerala, India, 2007), Chap. 5, pp. 103–150.
[8] Th. Anker, M. Albiez, R. Gati, S. Hunsmann, B. Eiermann, A. Trombettoni, and M. K. Oberthaler, Phys. Rev. Lett. **94**, 020403 (2005).
[9] J. D. Joannopoulos, R. D. Meade, and J. N. Winn, *Photonic Crystals: Molding the Flow of Light* (Princeton University Press, Princeton, NJ, 1995).
[10] Z. Shi and J. Yang, Phys. Rev. E **75**, 056602 (2007).
[11] T. J. Alexander, E. A. Ostrovskaya, and Y. S. Kivshar, Phys. Rev. Lett. **96**, 040401 (2006).
[12] D. N. Christodoulides and E. D. Eugenieva, Phys. Rev. Lett. **87**, 233901 (2001).
[13] J. Yang and Z. Musslimani, Opt. Lett. **28**, 2094 (2003).
[14] B. B. Baizakov, B. A. Malomed, and M. Salerno, Europhys. Lett. **63**, 642 (2003).
[15] D. N. Neshev, T. J. Alexander, E. A. Ostrovskaya, Y. S. Kivshar, H. Martin, I. Makasyuk, and Z. Chen, Phys. Rev. Lett. **92**, 123903 (2004).
[16] J. W. Fleischer, G. Bartal, O. Cohen, O. Manela, M. Segev, J. Hudock, and D. N. Christodoulides, Phys. Rev. Lett. **92**, 123904 (2004).
[17] C. Lou, X. Wang, J. Xu, Z. Chen, and J. Yang, Phys. Rev. Lett. **98**, 213903 (2007).
[18] E. A. Ostrovskaya and Y. S. Kivshar, Phys. Rev. Lett. **93**, 160405 (2004).
[19] R. Fischer, D. Trager, D. N. Neshev, A. A. Sukhorukov, W.

Krolikowski, C. Denz, and Y. S. Kivshar, Phys. Rev. Lett. **96**, 023905 (2006).
[20] G. Bartal, O. Manela, O. Cohen, J. W. Fleischer, and M. Segev, Phys. Rev. Lett. **95**, 053904 (2005).
[21] X. Wang, Z. Chen, J. Wang, and J. Yang, Phys. Rev. Lett. **99**, 243901 (2007).
[22] Y. V. Kartashov, V. A. Vysloukh, and L. Torner, Phys. Rev. Lett. **93**, 093904 (2004).
[23] X. Wang, Z. Chen, and P. G. Kevrekidis, Phys. Rev. Lett. **96**, 083904 (2006).
[24] M. J. Ablowitz, B. Ilan, E. Schonbrun, and R. Piestun, Phys. Rev. E **74**, 035601(R) (2006).
[25] D. E. Pelinovsky, A. A. Sukhorukov, and Y. S. Kivshar, Phys. Rev. E **70**, 036618 (2004).
[26] D. Neshev, E. Ostrovskaya, Y. Kivshar, and W. Krolikowski, Opt. Lett. **28**, 710 (2003).
[27] J. Wang and J. Yang, Phys. Rev. A **77**, 033834 (2008).
[28] D. Song, C. Lou, L. Tang, X. Wang, W. Li, X. Chen, K. J. Law, H. Susanto, P. G. Kevrekidis, J. Xu, and Z. Chen, Opt. Express **16**, 10110 (2008).
[29] N. G. Vakhitov and A. A. Kolokolov, Izv. Vyssh. Uchebn. Zaved., Radiofiz. **16**, 1020 (1973) [Radiophys. Quantum Electron. **16**, 783 (1973)].
[30] M. I. Weinstein, Commun. Pure Appl. Math. **39**, 51 (1986).
[31] M. Grillakis, Commun. Pure Appl. Math. **41**, 747 (1988).
[32] C. K. R. T. Jones, J. Differ. Equations **71**, 34 (1988).
[33] Y. S. Kivshar and G. P. Agrawal, *Optical Solitons: From Fibers to Photonic Crystals* (Academic, San Diego, 2003).
[34] Y. Sivan, G. Fibich, B. Ilan, and M. I. Weinstein, Phys. Rev. E **78**, 046602 (2008).
[35] N. Akhmediev, A. Ankiewicz, and R. Grimshaw, Phys. Rev. E **59**, 6088 (1999).
[36] J. Yang, New J. Phys. **6**, 47 (2004).
[37] M. Oster and M. Johansson, Phys. Rev. E **73**, 066608 (2006).
[38] J. Yang, I. Makasyuk, A. Bezryadina, and Z. Chen, Stud. Appl. Math. **113**, 389 (2004).
[39] F. Dalfovo, S. Giorgini, L. P. Pitaevskii, and S. Stringari, Rev. Mod. Phys. **71**, 463 (1999).
[40] B. B. Baizakov, V. V. Konotop, and M. Salerno, J. Phys. B **35**, 5105 (2002).
[41] J. Yang and T. I. Lakoba, Stud. Appl. Math. **118**, 153 (2007).
[42] S. Vlasov, V. Petrishchev, and V. Talanov, Radiophys. Quantum Electron. **14**, 1062 (1971).
[43] D. E. Pelinovsky, V. V. Afanasjev, and Y. S. Kivshar, Phys. Rev. E **53**, 1940 (1996).
[44] J. Yang, J. Comput. Phys. **227**, 6862 (2008).
[45] N. K. Efremidis, J. Hudock, D. N. Christodoulides, J. W. Fleischer, O. Cohen, and M. Segev, Phys. Rev. Lett. **91**, 213906 (2003).
[46] T. R. Akylas and Y. Cho, Philos. Trans. R. Soc. London, Ser. A **366**, 2761 (2008).